Discrimination and analysis of interactions in non-contact Scanning Force Microscopy

Elisa Palacios-Lidón and Jaime Colchero

Facultad de Quimica, Departamento de Física, Universidad de Murcia, E-30100 Murcia.

A method for the separation and quantitative characterization of the electrostatic and Van der Waals contribution to tip-sample interaction in non-contact Scanning Force Microscopy is presented. It is based on the simultaneous measurement of cantilever deflection, oscillation amplitude and frequency shift as a function of tip-sample voltage and tip-sample distance as well as on advanced data processing. Data is acquired at a fixed lateral position as interaction images with the bias voltage as fast scan and tip-sample distance as slow scan. Due to the quadratic dependence of the electrostatic interaction with tip-sample voltage the Van der Waals force can be separated from the electrostatic force. Using appropriate data-processing the Van der Waals interaction, the capacitance as well as the contact potential can be determined as a function of tip-sample distance from the force as well as from the frequency shift data. The measurement of resonance frequency shift yields very high signal to noise ratio and the absolute calibration of the measured quantities, while the acquisition of cantilever deflection allows the determination of tip-sample distance. The separation and quantitative analysis of Van der Waals and electrostatic interaction as proposed in the present work results in precise and reproducible measurement of tip-sample interaction that will significantly improve the interpretation of SFM data and will substantially contribute to the characterization of nanoscale properties by SFM.

I. INTRODUCTION

As scientific and technological interest focuses on increasingly smaller length scales, tools for visualizing and characterizing nanoscale systems are needed. An important technological step towards this goal is the development of techniques that allow precise and quantitative analysis of materials on a nanometer scale. In this context, Scanning Probe Microscopy, and in particular Scanning Force Microscopy (SFM) [1] has proved to be a very powerful tool for Nanotechnology. SFM allows not only the visualization of surfaces on a nanometer scale, but also its modification and the characterization of material properties. SFM is based on the interaction of a very sharp tip with the sample to be studied. Therefore, a deep understanding of tip-sample interaction is fundamental in SFM. A variety of forces may act between tip and sample: dispersion, electrostatic, chemical, elastic as well as adhesion and friction forces. In addition, when tip and sample are composed of magnetic materials, also magnetic forces act. Each of these forces in principle opens the way for measuring the corresponding physical property of the sample.

The variety of different forces - and thus different material properties - that can be measured is one of the reasons for the great versatility of SFM. Correspondingly, at present SFM is used very successfully and extensively in a variety of scientific areas. However, we believe that it is still not the precise and quantitative tool required by the Nanotechnology community. One of the difficulties for quantitative measurements with SFM is -in our opinion- precisely the wealth of interactions that may act in a SFM set up. Since, a priory, only the total force is measured, it is difficult to discriminate between the contributions of the different kind of forces. However, to obtain quantitative measurements and for a complete characterization of material properties on an nanometer scale, as well as in general for the correct interpretation of SFM experiments, the determination of the origin and the relative strength of the measured forces is fundamental.

Due to its importance, tip-sample interaction has been the topic of a variety of studies. Some of these studies are focused on the modeling and analysis of the dynamics of the oscillating tip within the (non-linear) surface potential[2, 3, 4, 5], while others are devoted to the physics of the interaction itself[6, 7, 8]. In this context, the modeling and measurement of electrostatic interaction within a SFM set-up has received particular attention[9, 10, 11, 12]. A variety of methods have been used to experimentally characterize the interaction between tip and sample in a SFM-setup. The simplest is based on the acquisition of force versus distance ($FvsD$) curves[13]. This mode measures the static deflection of the cantilever as tip-sample distance is varied and is easy to implement but is not sensitive enough to analyze weak forces. A more precise method measures variations of the oscillation of the cantilever, that is, of its amplitude, phase or resonance frequency (amplitude, phase or frequency vs. distance curves). Dynamic methods are more sensitive due to signal enhancement induced by the resonance of the cantilever[14]. More sophisticated methods are based on the multidimensional acquisition of data, where the interaction is measured not only as a function of tip-sample distance, but as a function of at least a second variable. In one of those modes the mechanical spectrum of the cantilever is determined as a function of tip-sample distance, in this case the second variable is the excitation frequency. The oscillation of the tip is induced either by thermal fluctuation[15], or by external excitation[16, 17, 18].

SFM experiments can be performed in Ultra High Vacuum (UHV) conditions or in liquids and air. While the first

kind of experiments are more demanding, the latter are more difficult to understand due to less controlled surface conditions: in air adsorbed liquid films and different kind of contamination may complicate data interpretation. Moreover, while in UHV conditions the tip can approach the surface as near as atomic distances and "feel" chemical interactions, in air the minimum tip-sample distance is about one magnitude larger, since the tip snaps to the surface not due to the instability produced by typical surface potentials, but due to the (spontaneous) formation of liquid necks[18], occurring at distances between 2 and 5 nm. Correspondingly, quantitative determination of tip-sample interaction in air is more challenging since signals are typically weaker and interaction data has to be analyzed and interpreted with care[19, 20]. In many cases the correct determination of tip-sample distance and of the "true" non-contact regime is crucial[21].

In the "true" non-contact regime dispersion forces, which are always present, and electrostatic forces, which are the strongest forces and have long interaction range, are the most relevant forces in a typical SFM set up. Separation of these two kind of interactions is fundamental for a better understanding of tip-sample interaction, for adjusting of optimum imaging conditions as well as for the quantitative determination of material properties on a nanometer scale. In principle, as recognized in previous works, variation of tip-sample bias results in turning "on" and "off" the electrostatic interaction, allowing to separate the dispersion interaction from the electrostatic interaction. In fact, to experimentally verify the quadratic dependence of tip-sample interaction on on tip-sample voltage and to characterize the dielectric properties of different samples Hu et al.[22] have acquired interaction versus voltage curves. In a similar approach, Guggisberg et al.[23] have measured tip-sample interaction as a function of tip-sample voltage and tip-sample distance to determine and compensate the contact potential between tip and sample. The goal of that work performed in ultra high vaccum was the precise discrimination and control of dispersion and electrostatic interactions in order to measure short ranged chemical forces. In the present work we pretend to further develop these techniques for separation and measurement of electrostatic and dispersion interaction. As in the works just discussed data is acquired as a function of tip-sample distance and of tip-sample voltage. The corresponding experimental data sets are stored and visualized as "interaction images". The to obtain a complete characterization of tip-sample interaction cantilever deflection (force), oscillation amplitude as well as frequency shift are acquired simultaneously and processed using appropriate data processing algorithms. The measurement of resonance frequency shift yields very high signal to noise ratio and the absolute calibration of the measured quantities, acquisition of oscillation amplitude allows to recognize the "true" non-contact regime, and from the cantilever deflection tip-sample distance is determined. Precise values for the dispersion interaction, the contact potential and the tip-sample capacity[24] are obtained as a function of tip-sample distance. Furthermore, this method allows to characterize parameters such as the tip radius and the tip-sample distance. We note that this method requires no previous information about the electric properties of the tip-sample system -and in particular about the contact potential- since this information is obtained "self-consistently" by the algorithm processing the interaction images. In particular for experiments performed in air, but also for UHV applications we are convinced that the method presented in this work will result in improved data acquisition and data interpretation. Moreover, we believe that this method will contribute to obtain the profound understanding of tip-sample interaction needed to quantitatively determine electrostatic properties of samples on a true nanometer scale.

II. THEORETICAL BACKGROUND

In a typical SFM experiment tip-sample interaction $I(d)$ (that is, energy) is not measured directly. Instead the force $F(d) = -I'(d)$ or the resonance frequency are determined from experiment. The resonant frequency of the tip-sample system and the curvature $I''(d)$ of the interaction potential are related by

$$v_0(d) = \sqrt{\frac{c_{lev} + I''(d)}{m_{eff}}}/(2\pi) \simeq v_{00}(1 + \frac{1}{2}\frac{I''(d)}{c_{lev}})$$ (1)

with v_{00} free resonance frequency of the cantilever, c_{lev} its force constant and m_{eff} the effective mass of the cantilever. We note that this relation is only correct if the oscillation amplitude is sufficiently small in order to avoid non-linearities of the interaction[25]. The approximation is valid as long as $I''(d) \ll c_{lev}$ or, equivalently, for small shifts $\Delta v_0(d) = v_{00} - v_0(d) \ll v_{00}$ of the resonance frequency. For a detailed discussion of the mechanical behavior of a SFM setup see Duerig[26].

To simplify the argumentation, in the context of the present work we will assume a homogeneous sample. We note, however, that the results discussed here are also relevant for heterogeneous samples as long as the sample is "locally" homogeneous, which means that the material properties of the sample are homogeneous on a length scale larger than the resolution of the SFM-system, that is, its effective aperture function. We will also assume that in the

true non-contact regime[21] tip-sample interaction is governed only by dispersion and electrostatic interaction:

$$I(d) = I^{dis}(d) + I^{estat}(d) \tag{2}$$

with $I^{estat}(d)$ electrostatic interaction and $I^{dis}(d)$ dispersion interaction. From a fundamental point of view, both kind of interactions can be considered ultimately of electronic origin. While the electrostatic interaction arises "directly" from charges, dispersion forces arise "indirectly" through the residual interaction of fluctuating dipoles within matter (Van der Waals forces) or fluctuating electric fields in vacuum (Casimir forces)[27]. Van der Waals and Casimir forces are of quantum mechanical origin. In the context of the present work, we will assume that the dispersion forces within a SFM-setup are well described by the relation[7, 28]

$$F^{vdW}(d) = \frac{A_{tms}\,R}{6\,d^2} \tag{3}$$

which describes the Van der Waals force between a tip of radius R and the sample surface by means of the Hamaker constant A_{tms} (tip interacting with sample through medium, see Israelachvili[28] for a detailed discussion).

If tip and sample are electrical conductors the electrostatic force between tip and sample can be written as a surface integral over the electric field on the sample surface[30]. In addition, the electric field lines can be approximated by segments of circles connecting tip and sample. To a good approximation, the electric potential decays linearly along these circular segments. Within this approach, the electrostatic force between tip and sample can be calculated as [29]:

$$F(d) = \int_S dS\,\frac{\varepsilon_0}{2}\,E(x,y,d)^2 \simeq \frac{\varepsilon_0 U_0^2}{2} \int_S dS\,\frac{1}{a(x,y,d)^2} \tag{4}$$

where $E(x,y,d)$ is the electric field on the surface for a certain tip-sample distance d, U_0 is the effective voltage between tip and sample and $a(x,y,d)$ the arc length of the circular segment coming from the probe and ending on a point (x,y) of the surface. When nanoscale dielectric systems are adsorbed on a conducting surface, it can be shown within a perturbative approach[31] that tip-sample interaction depends also on the electrical properties of these systems, which are the objects to be characterized by SFM.

Many SFM experiments are performed with a conducting or semiconducting tip in order to control its potential. It would seem reasonable to assume that grounding the tip with respect to the sample surface would imply vanishing of electrostatic forces. This is, however, only correct if the work function (or contact potential) of tip and sample are equal. Otherwise, differences in work function induce transfer of charges that result in electrostatic fields and thus, according to equation 4, in electrical forces even if no external bias is applied. The electrostatic force between tip and sample is therefore a quadratic function of tip voltage with its minimum shifted by an amount U_{cp} with respect to the origin due to contact potential difference[32, 33]:

$$F_{el}(d) = C'(d)(U_{tip} - U_{cp})^2/2 \tag{5}$$

where $C'(d)$ is the derivative of the tip-sample capacity. For a conductive tip and sample, this derivative of the capacitance can be estimated by the surface integral of equation 4

$$C'(d) = \varepsilon_0 \int_S dS\,\frac{1}{a(x,y,d)^2} \tag{6}$$

For the case of Van der Waals interaction we assume a specific tip geometry -namely a parabola described by a tip radius R, see relation 3- while for the case of the electrostatic interaction equation 4 is generic, that is, in principle any tip-sample geometry can be described using an appropriate tip-sample capacity $C(d)$. This different treatment is justified because of the different distance dependencies of Van der Waals and electrostatic interactions. Due to its faster decay Van der Waals interaction is less sensitive to the large scale geometry of the probe (see Argento et. al.[7] and Colchero et. al.[34] for a more detailed discussion). In fact, for the experiments described in the present work we find that the commonly used approximation - $C(d) = 2\pi\,\varepsilon_0\,R\ln(d)$ - for the tip-sample capacitance[35] does not describe tip-sample interaction satisfactory within our experimental error. Therefore, the relation

$$C(d) = 2\pi\varepsilon_0 R\ln\left(\frac{d}{d + R(1 - \sin\vartheta_0)}\right) \tag{7}$$

for the tip-sample capacity will be used, which results from modeling the tip as a truncated cone of opening angle ϑ_0 ending smoothly in a spherical tip apex of radius R (see Hudlet et. al. [29] for a detailed discussion of this model probe tip).

As a general result from this theoretical section we conclude that for a fixed distance d_0 the total tip-sample interaction as a function of voltage and tip-sample distance is of the form

$$i(U, d_0) = \alpha(d_0) + \gamma(d_0)(U - \kappa(d_0))^2/2 \qquad (8)$$

where the constant term α describes the Van der Waals interaction, γ the curvature of the parabola induced by electrostatic interaction and κ the position of the minimum. Note that this general relation applies to the force as well as for the force gradient, and thus also for the resonance frequency. This quadratic dependence of tip-sample interaction on voltage is essentially the basis for the separation of Van der Waals and electrostatic interaction in this work (see also Hu et al. [22] as well as Guggisberg et al. [23]).

III. EXPERIMENTAL METHOD

Usually either the force, the resonance frequency or the oscillation amplitude are measured to characterize the tip-sample interaction. In the present work, all three quantities are measured simultaneously. By measuring the force the first derivative of the interaction (equation 2) is determined experimentally while the resonance frequency is related to the second derivative of the interaction. As will be discussed in more detail below, the method presented here allows the precise determination of all parameters relevant for tip-sample interaction. By measuring a family of curves $i(U, d_0)$ as a function not only of tip voltage U but also of tip-sample distance *interaction images* $i(U, d)$ can be obtained. Each horizontal line can then be adjusted to the parabola defined by equation 8 to obtain, for each tip-sample distance, the contribution of the Van der Waals interaction, the contact potential and the tip-sample capacitance. From a whole *interaction image* $i(U, d)$ three curves are obtained, one, $\alpha(d)$, characterizing the Van der Waals interaction as a function of distance, another one, $\gamma(d)$, describing the capacitance of the tip-sample system as a function of distance and the third one, $\kappa(d)$, corresponding to the contact potential as a function of tip-sample distance.

A. Data acquisition

Figure 1 schematically shows the experimental implementation of the setup used to acquire the *interaction images*. The experiments were performed with a NanoTec SFM system composed of SFM head, high voltage controller and PLL/dynamic measurement board[36]. For our experiments, we find that cantilevers with long tips, located at its very end are ideal, since these kind of SFM probes minimize the effect of the interaction between the sample and the (macroscopic) cantilever, which can result in uncontrolled electrostatic interaction[37] and (long-range) viscous forces[40] that decrease the quality factor of the oscillation and thus the sensitivity in dynamic detection modes. Olympus OMCL-AC-type cantilevers have been used in all experiments[41]. The *interaction images* were acquired using the "3D-Mode"[42], which allows fast switching from normal imaging to a series of extended acquisition modes. "3D-Mode" is a generalized acquisition mode where data -that is, some input channel- is acquired as a function of two output channels that are user selected: $datain = datain(output_1, output_2)$. "3D-Mode" images are acquired in a raster scan mode where one channel is varied "fast" at a fixed value of the "slow" output, then the "slow" output is varied by one step and a new line of data is acquired by varying the "fast" output. For the experimental data shown here, the "3D-Mode" was set in order to have the tip voltage as fast scan and the tip-sample distance as slow scan, that is, the tip-sample voltage is ramped fast to acquire, for each distance, interaction data as a function of tip-sample voltage while tip-sample distance is varied slowly to bring the tip into and out of contact with the sample[43, 44]. For each set of experiments, the normal force, the frequency shift and the oscillation amplitude are measured as a function of tip-sample voltage and tip-sample distance.

To measure the resonance frequency of the tip-sample system the cantilever is excited near its resonance frequency by a small piezoelectric element and a Phase Locked Loop (PLL)[14] is used to track the resonance frequency as bias voltage and tip-sample distance are varied. The use of a PLL-circuit allows the direct measurement of the resonance frequency in Hertz, and thus the determination of interaction data in physically meaningful units. Calibration of force data was performed using the nominal force constant of the cantilevers to convert deflection into force and by calibrating the photodiode signal with a $FvsD$ curve[45]. Typical oscillation amplitudes were 0.1 to 2.5nm (0.2 to 5nm peak to peak). The lower threshold of the oscillation is set by thermal noise of the cantilever, while the higher value was chosen in order to avoid non-linearities of the interaction. As a reasonable criterion we have chosen amplitudes that are smaller than the minimum tip-sample distance at the snap to contact point.

B.   Data processing

Data is processed as follows: in a first step, each force line is averaged to obtain a *FvsD* curve. This *FvsD* curve is then analyzed by means of an appropriate algorithm that determines the snap to contact point in order to separate the contact and non-contact regimes of the curve. We note that, since data is acquired in air, the snapping instability is induced by the spontaneous condensation of a liquid neck between tip and sample at rather large distances of 2-5nm[18, 19]. In order to obtain meaningful interaction data the jump distance, which can only be measured if the cantilever deflection (force) is acquired, has to be taken into account. From the *FvsD* curve the snapping distance is measured and the position of the surface as well as the true tip-sample distance is determined. All curves calculated from the same set of *interaction images* are then shifted horizontally by a constant amount corresponding to the position of the surface as "seen" by the *FvsD* curve. Then, the origin of the horizontal axis (piezo displacement) corresponds to the displacement of the piezo where the cantilever would touch the surface if no attractive forces where present. In a second step, force and frequency data corresponding to the non-contact regime, that is, before the snapping instability, are adjusted to a quadratic function according to equation 8. From the force *interaction image* three curves $f^{vdW}(d)$, $C'(d)$ and $U_{cp}^{force}(d)$ are obtained describing the Van der Waals force, the first derivative of the tip-sample capacitance, and the contact potential as "seen" by the force data. In the same way the frequency *interaction image* yields three corresponding curves $\Delta\omega_0^{vdW}(d)$, $C''(d)$ and $U_{cp}^{freq}(d)$; the frequency shift induced by the Van der Waals interaction, the second derivative of the capacitance and the contact potential as "seen" by the frequency data. Finally, the three most relevant curves - $\Delta\omega_0^{vdW}(d)$, $C'(d)$ and $C''(d)$ - are compared with the relations

$$\Delta\omega_0^{vdW}(d) = \frac{1}{2}\frac{\omega_{00}}{c_{lev}}V''_{vdW}(d) = \frac{1}{6}\frac{\omega_{00}}{c_{lev}}\frac{A\ R_{vdW}}{(d - d_0^{vdW})^3} \tag{9}$$

$$C'(d) = 2\pi\varepsilon_0 R_{estat}\frac{R_{estat}(1 - \sin(\vartheta))}{(d - d_0^{est1})\,(d - d_0^{est1} + R_{estat}(1 - \sin\vartheta)} + b_1 \tag{10}$$

$$C''(d) = 2\pi\varepsilon_0 R_{estat}\left(\frac{1}{(d - d_0^{est2})^2} - \frac{1}{(d - d_0^{est2} + R_{estat}(1 - \sin\vartheta))^2}\right) + b_2 \tag{11}$$

which describe the frequency shift expected for a pure Van der Waals interaction of a tip with radius R_{vdW}, and the first and second derivatives of the capacitance predicted for a truncated cone ending in a spherical tip apex of radius R_{estat}. The two constants b_1 and b_2 are introduced to account for the possible effect of long range contributions to the electrostatic interaction due to the tip cone or the cantilever (see [37, 38, 39]). Each adjustment is allowed to find its own tip radius. In addition, each adjustment is allowed to find the best value for d_0. Note that the parameters d_0 represent mathematically the poles of the interaction, that is, the position where the interaction diverges. From a physical point of view, these poles correspond to the position of the surface. Complete agreement with the surface position obtained from the *FvsD* curve would require $d_0 = 0$, since, as described previously, all curves have been shifted to this position. From a physical point of view different tip radii R and different distances d_0 imply that the corresponding curves "see" different tips and different surface positions.

IV.   EXPERIMENTAL RESULTS

Measurements have been performed on a variety of samples under different experimental conditions. As representative cases two experiments performed on a Au(111) surface are presented here, one taken with a highly doped silicon tip at a relatively large oscillation amplitude of 2.5nm (5nm peak to peak), and another one taken with a Pt-coated tip at a significantly lower amplitude of 1nm. We consider the first case to be representative for typical experiments in SFM and Electrostatic Force Microscopy, while the second case is closer to the ideal situation where tip and sample are truly metal surfaces and the oscillation amplitude is sufficiently small to neglect non-linear effects in the tip-sample interaction.

Figure 2 shows a typical set of force and frequency *interaction images* as well as an oscillation amplitude image acquired on an Au(111) surface with a Si tip[41] in ambient air (temperature $\simeq$22°C, relative humidity $\simeq$50%). These images show pure raw data, no plane or other form of data-processing has been applied. The lower part of the images corresponds to small tip-sample distances (near the surface), the lowest lines that appear flat correspond to data taken with tip and sample in mechanical contact. In this regime, none of the *interaction images* show the quadratic dependence on the tip-sample voltage that is visible in the non-contact regime. The frequency shift image is completely

saturated because the elastic interaction drives the resonance frequency of the tip-sample system far away from the free resonance frequency[46]. In the normal force the quadratic dependence is observed for small and large tip-sample distances, while in the amplitude and in the frequency *interaction image* the quadratic dependence is observed only very near the surface ($\lesssim$10nm). As will be discussed in more detail below, this indicates a very short interaction range for the frequency and the amplitude signal. The parabolic dependence of the amplitude is attributed to increased dissipation in the tip-sample system, but at the moment the precise origin of this dissipation is still unknown. In the normal force image the jump to contact is recognized as a step towards lower force values followed by a continues increase of the normal force.

Figure 3 shows the *FvsD* curve obtained by averaging each line of the force *interaction image*. In addition, the amplitude image has been processed to calculate the oscillation amplitude for each tip-sample distance, which allows to determine the upper and lower turning point of the tip motion during oscillation shown in figure 3. As discussed above, the oscillation amplitude ($\simeq 2.5$ nm) has been chosen to be smaller than the distance corresponding to the jump to contact regime. The mean jump distance measured from the force curve is about $\overline{d}_{jump} \simeq 4$ nm, however, we believe that the effective jump distance is

$$d_{eff} = \overline{d}_{jump} - a_{osci}$$

where $a_{osci} \simeq 2$ nm is the oscillation amplitude just before the jump to contact instability. The effective jump distance is then about 2nm. The reasoning behind this correction is that the jump to contact is believed to be induced by condensation of liqid necks at the lowest turning point of the oscillation, that is, at the smallest tip-sample distance[18]. Jump to contact then occurs at the smallest tip-sample distance rather than from the mean tip-sample distance. The force curve shows very low adhesion and very little hysteresis: the area enclosed during the whole forward and backward cycle is the energy dissipated during the acquisition process and corresponds to about 10^{-17} J ($\simeq 60$ eV). Acquisition of this curve is therefore quite gentle. The measured adhesion force allows to estimate the product of tip radius and contact angle according to[28, 47]

$$F_{ad} = 4\pi\gamma R \cos(\varphi)$$

where R is the tip radius, γ the surface energy of water and φ the effective contact angle of water on the tip-sample system. With a force constant $c = 2$ N/m and assuming a wetting sample[48], that is, a contact angle $\varphi \simeq 0 - 30°$, we obtain an estimated tip radius of 10-15nm, in good agreement with results obtained from the non-contact measurements to be discussed below.

The force curve together with the frequency and amplitude distance behavior allows to separate four regimes that can be present during tip-sample approximation (see also Fig. 3): first, a true non-contact regime where the cantilever essentially oscillates with its free resonance frequency, second, a "tapping non-contact" regime where the oscillation amplitude decreases even though no mechanical contact between tip and sample is formed, third, an intermittent contact regime where the tip still oscillates and dynamically touches the surface, and forth a continuous contact regime where the cantilever no longer oscillates. In our experiments we use rather soft cantilevers at small oscillation amplitudes, therefore we do not observe the intermittent contact regime (see figure 3), in this case the oscillation stops as soon as the tip mechanically touches the surface for the first time since the adhesion force is larger than the restoring force of the cantilever[49, 50]. With very small oscillation amplitudes also the second "tapping non-contact" regime may not be observed, then the tip directly snaps on to the surface before any significant dissipation is detected.

In the non-contact regimes the *interaction images* are processed as discussed in the previous section to obtain, for each *interaction image*, three curves describing the Van der Waals interaction, the capacitance and the surface potential. Figure 4 shows the result of this process for the *interaction images* shown in Fig. 2. The graphs in Fig. 4a, 4c and 4e represent the curves obtained from the force *interaction image* while the graphs in Fig. 4b, 4d and 4f have been obtained from the frequency *interaction image*. The Van der Waals curve obtained from the force *interaction image* essentially reproduces the *FvsD* curve obtained by simple averaging, a small difference is due to the effect of the electrostatic interaction: while the curve in Fig. 3 is a mixed electrostatic/Van der Waals curve[51], the curve in Fig. 4a is a "true" Van der Waals *FvsD* curve. The parameters obtained from the adjustment of the experimental data to the relations 9-11 are summarized in Table 1.

To investigate the precision of the method described in the present work two test have been made. First, the data describing the interaction has been adjusted to the relations 9 and 11 allowing the fit to find the exponents n_{vdW} (which was n_{vdW} =3 in relation 9) and n_{el} (which was n_{el} =2 in relation 11, in the present context only the first term with the pole $1/(d - d_0^{est2})^2$ is considered relevant). The results of the corresponding fits are listed in table 2, confirming that the data indeed reproduces correctly the exponent of Van der Waals as well as electrostatic interaction.

For the second test the data corresponding to tip-sample capacity (that is, $C''(d)$) was adjusted using two different functions in order to check whether the data is able to "see" the difference. One relation is obtained from the usual spherical approximation which gives $C''(d) = 2\pi \epsilon_0 R/d^2$, and the second relation is obtained using the more

sophisticated model leading to equation 11. In this second model, the cone angle was fixed to $\vartheta_0 = 20°$, as specified by the manufacturer. Both models therefore have the tip-radius as only free parameter. The corresponding fits together with their errors are shown in Fig. 4d. Even though both fits yield parameters that are compatible one with the other, the first model for the tip-sample capacitance shows a clear tendency of the error not observed in the second one.

Figure 5 shows the result of the processing of force and frequency *interaction images* as well as an oscillation amplitude image acquired on an Au(111) surface with a Pt-coated Silicon tip. As in the previous case, data was acquired in ambient air. The graph in Fig. 5a, and 5c represent the curves obtained from the force *interaction image* while the graph in Fig. 5b and 5d have been obtained from the frequency *interaction image*. Table 3 summarizes the values for tip radius and surface position obtained from the adjustment of the curves 5b-5d to the relations 9-11. Due to the lower oscillation amplitude (1nm), no "tapping non-contact" range is observed. The mean jump distance is again about 3.5 nm, and the effective jump distance is 2.5 nm, somewhat larger than in the previous case. The results obtained from this second experiment are similar to those obtained in the first one, as can be verified by comparing the parameters for tip radius and surface position listed in Table 1 and 3. The slightly higher noise level in the second experiment as compared to the first one is attributed to the lower oscillation amplitude. Nevertheless, at present we believe that for low oscillation amplitudes our measurements are limited by technical noise rather than fundamental limits such as shot noise or thermal movement of the cantilever. In the case of the Si-tip, the Van der Waals radius ($R^{vdW} = 5.8\pm0.4$nm) is considerably smaller than the two electrostatic radii ($R^{estat1}=12\pm1$nm, $R^{estat2}=21\pm4$nm). Moreover, these two electrostatic radii do not agree within the measured experimental error. One possible explanation for this may be that, at the level of precision of the method, the Si-tip is not a sufficiently ideal tip due to the presence of oxide layers on its surface and/or to band bending effects. In the case of the Pt-tip, the Van der Waals radius ($R^{vdW} = 14\pm5$nm) as well as both electrostatic radii ($R^{estat1}=16\pm12$nm, $R^{estat2}=21\pm6$nm) are compatible one with another, indicating that Van der Waals and electrostatic interaction "see" the same geometry of the tip. Finally, we note that the Van der Waals radii obtained for the Si-tip and for the Pt-tip are in good agreement with the nominal values of the manufacturer: the Si-tip has a nominal radius better than 10nm, while the Pt-tip, consisting of a thin 10-15nm thin Pt-film on the same kind of Si-tip should have a tip radius of 15-25nm[41].

As a general result from both experiments we find that the data obtained from the frequency image has less dispersion and less error in the estimation of the parameters describing the tip-sample interaction. The noise in the data characterizing the surface potential decreases for small tip-sample distances only for the data obtained from the frequency *interaction image* (compare figures 4f and 4e). The offset b_1 obtained from the force interaction image is clearly different from zero, in fact, it accounts for almost 50% of the electrostatic interaction at the smallest tip-sample distance, while the corresponding offset b_2 obtained from the frequency *interaction image* is essentially compatible with $b_2 = 0$. These offsets reflect the amount of electrostatic interaction that does not change on a length scale comparable to the distance sampled by an *interaction image* (100nm). Therefore, as discussed previously, we conclude that the force signal with the large value of the offset b_1 has a significant long range component of electrostatic interaction while the frequency, with its vanishing offset b_2, has a truly short range behavior. As described in detail elsewhere[34], the long range component of the electrostatic interaction is due to the mesoscopic tip cone or the macroscopic cantilever, while the short range interaction is induced by the nanoscopic tip apex, usually described by means of an (effective) tip radius. In the frequency (that is, force gradient) signal, the long range component of the interaction is "derived away" and only the interaction with the nanoscopic tip apex is relevant. In our opinion, this explains the large value of b_1 obtained from the force *interaction image* as compared to the vanishing of b_2 obtained from the frequency *interaction image*.

For small indentation forces, the experiments described here are quite reproducible. This is seen in Fig. 6, which shows the result of processing three different *interaction images* taken consecutively at a same spot of an Au(111) surface. The corresponding *FvsD* curves obtained from force *interaction images* are shown with approach and retraction cycle (Fig. 6a). The second derivative of the capacitance as well as the contact potential were obtained from frequency *interaction images* and only approach curves are presented. Within the experimental error the three indentations lead to essentially the same results. In particular, the *FvsD* curves are almost absolutely equivalent, the three curves show not only the same jump to contact distance and the same adhesion force, also the details of how the tip-sample contact breaks are very similar. Images taken before and after the acquisition of these curves showed no variation of the surface, confirming that the surface was not modified during the indentation experiments. When thermal drift is sufficiently low, an even more gentle measurement of tip-sample interaction is possible by acquiring *interaction images* without bringing the tip into mechanical contact with the sample. Tip-sample distance can then in principle be estimated from the values of the poles d_0 of tip-sample interaction (see relations 9-11). In this case, the tip is maintained pristine. In particular when very sharp tips are used, this is a significant advantage over other techniques for measuring tip-sample interaction. In our opinion, the results shown in Fig. 6 demonstrate the potential and precision of the method. The method is sufficiently sensitive to detect possible variations of the tip-sample system, which may be detected in any of the measured parameters, that is, not only in the *FvsD* curve (and in particular in

the adhesion force), but also in the surface potential or in the capacitance of the tip-sample system.

V.   CONCLUSION

In the present work, the Van der Waals and electrostatic contribution to the interaction in a SFM set-up have been separated and analyzed quantitatively. The method described is based on the acquisition of *interaction images* where the force, the oscillation amplitude and the resonance frequency are acquired as a function of tip-sample distance and tip-sample voltage. Using appropriate processing algorithms, the Van der Waals interaction, the electrostatic interaction and the contact potential are determined from the force as well as from the frequency data. We note in this context that other methods for measuring tip-sample interaction do not directly allow the separation of Van der Waals and electrostatic interaction. In particular, when the materials of tip and sample are different -which is usually the case- contact potentials may significantly contribute to the total tip-sample interaction. If pure Van der Waals interaction is to be measured, the contact potential has to be compensated and if electrostatic interaction is measured, the contact potential has to be taken into account. With the method described here, Van der Waals interaction, electrostatic interaction - described by means of a tip-sample capacitance or some of its derivatives - and contact potentials are determined "self consistently", that is, the method automatically takes account of the effect induced by each of these three phenomena. More technically, our method assumes no prior information about the physical properties of the tip-sample system, instead it "finds" the combination of parameters corresponding to Van der Waals and electrostatic interaction that best describe the measured data.

Our experiments performed with (highly doped) semi-conducting as well as with metalized tips demonstrate the potential of the method and yield high precision, quantitative and reproducible interaction data. The high precision of the method is due to the fitting process which implies averaging of experimental data. Typically 100 to 1000 data points are acquired (one line of an *interaction image*) to obtain three physically relevant parameters, therefore the signal to noise ratio of these curves increases as compared to the usual acquisition of interaction versus distance curves. Assuming that data fitting increases the signal to noise ratio as $\sqrt{n}$, with n number of data points, the improvement of signal to noise ratio is about one order of magnitude. Another feature of the method presented is that the processing algorithms can be developed further to test whether the electrostatic interaction follows the quadratic dependence with bias voltage described by relation 5. This is particularly relevant for semiconducting tips or samples as well as for strong electric fields between tip and sample where departures from the quadratic behavior could be expected. In addition, also inhomogeneities of the tip surface potential could be recognized due to non-ideal behavior of the interaction with tip-sample voltage as well as due to a distance dependence of the measured surface potential (see also[34]).

We have shown that the technique is able to experimentally determine the exponent of the Van der Waals and the electrostatic interaction. In addition, the technique is also able to differentiate between two models for electrostatic tip-sample interaction, showing that an accurate description of electrostatic interaction needs to go beyond the simple sphere-sample approximation used generally.

We believe that the method presented in this work will significantly contribute to improve the measurement of interaction in a SFM setup and aid the correct interpretation of SFM experiments. In addition, an improved characterization of interaction will allow quantitative determination of material properties on a nanometer scale, an issue that recently is receiving more and more attention but that, in our opinion, still needs some important efforts from the SPM community.

VI.   ACKNOWLEDGMENTS

VII.   TABLES

curve	tip radius R	surface position d_0	offset b
force $F(d)$	$10 - 15nm$ (from F_{ad})	0 (by definition)	–
frequency $\nu(d)$	$R^{vdW} = 5.8 \pm 0.4nm$	$d_0^{VdW} = 3.1 \pm 0.2nm$	–
force-capacitance $C'(d)$	$R^{estat1} = 12 \pm 4nm$	$d_0^{estat1} = 2 \pm 2nm$	$b_1 = -(7 \pm 4) * 10^{-3}$
frequency-capacitance $C''(d)$	$R^{estat2} = 21 \pm 1nm$	$d_0^{estat2} = 1.2 \pm 0.9nm$	$b_2 = -(37 \pm 14) * 10^{-6}$

Table 1

Parameters describing tip-sample interaction obtained after processing the *interaction images* shown in Fig. 2, and the curves shown in Figs. 4b), 4c) and 4d). Data acquired with a Si-tip on an Au (111) surface. Resonance frequency: 73.67 kHz, force constant 2N/m, free oscillation amplitude 2.5 nm.

Curve	tip radius R	surface position d_0	exponent experiment	exponent theory
$\nu(d)$	$15 \pm 30nm$	$3 \pm 2nm$	3.3 ± 0.5	3
$C''(d)$	$17 \pm 1nm$	$2.2 \pm 0.2nm$	1.9 ± 0.5	2

Table 2

Parameters describing tip-sample interaction obtained after processing the *interaction images* shown in Fig. 2, and the curves shown in Figs. 4b), 4c) and 4d). In addition to the parameters R and d_0, also the exponents describing the variation with tip-sample distance in relations 11 and 9 were allowed to vary.

curve	tip radius R	surface position d_0	offset b
force $F(d)$	$10 - 15nm$ (from F_{ad})	0 (by definition)	–
frequency $\nu(d)$	$R^{vdW} = 14 \pm 5nm$	$d_0^{VdW} = 1.7 \pm 0.5nm$	–
force-capacitance $C'(d))$	$R^{estat1} = 16 \pm 12nm$	$d_0^{estat1} = 2.1 \pm 1.1nm$	$b_1 = -0.1 \pm 0.3$
frequency-capacitance $C''(d)$	$R^{estat2} = 21 \pm 6nm$	$d_0^{estat2} = 1.2 \pm 0.7nm$	$b_2 = -(1.7 \pm 1.3) * 10^{-4}$

Table 3

Parameters describing tip-sample interaction obtained after processing *interaction images* acquired with a Pt-tip on an Au (111) surface. Resonance frequency: 68.80 kHz, force constant 2N/m, oscillation amplitude 1 nm.
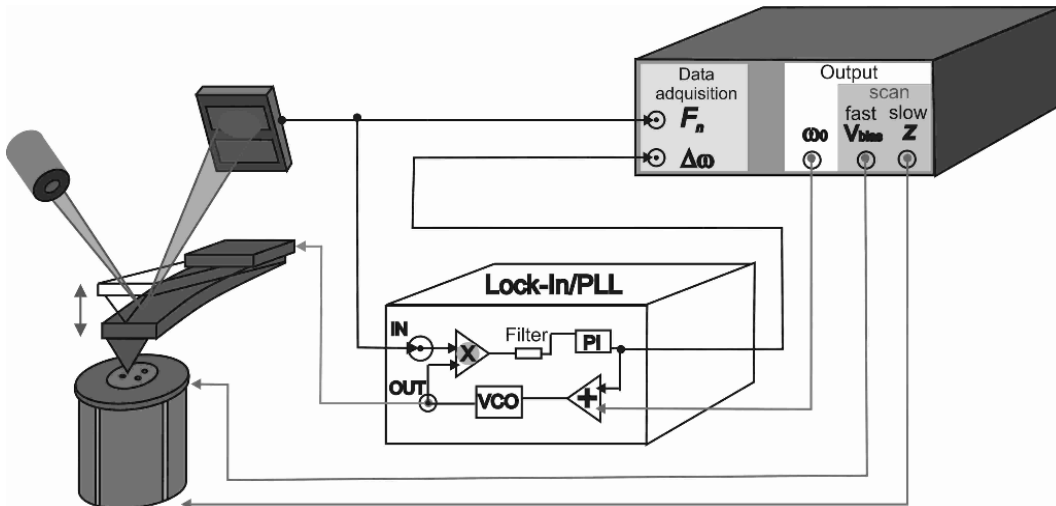
VIII.   FIGURE CAPTIONS

Figure 1

Schematic description of the experimental setup used to acquire "interaction images". The lateral position of the tip over the sample is fixed. The "fast" and "slow" outputs of the electronics are used to vary the tip-sample voltage and the tip-sample distance. A Phase Locked Loop is used to mechanically oscillate the tip-sample system always at resonance. Frequency shifts Δv are measured with respect to a reference frequency -usually the free resonance frequency- set by the electronic system. In our experiments, the force, the frequency shifts and the variation of oscillation amplitude induced by the tip-sample interaction are measured simultaneously.
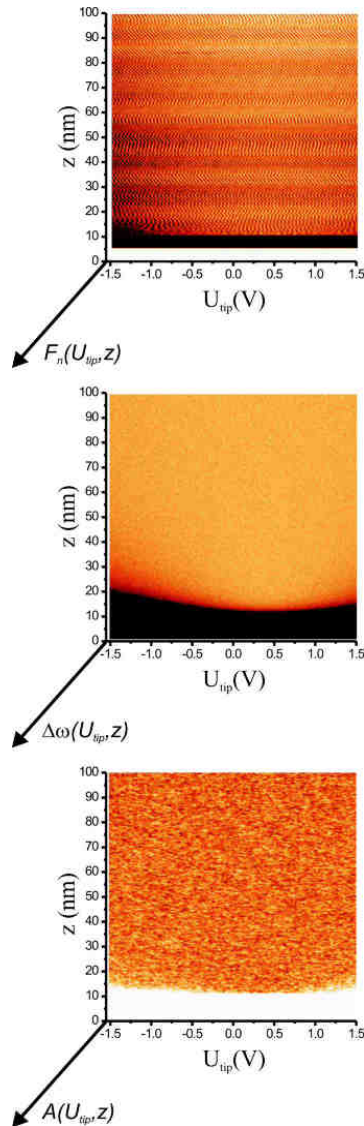

Figure 2

Typical set of interaction images acquired by varying the bias voltage ("fast" scan, corresponding to a horizontal scan line) and the tip-sample distance ("slow" scan, vertical direction). The upper part of the images corresponds to large tip-sample distances, the lower part to small distances. At the bottom of the images, tip and sample are in mechanical contact. Resonance frequency: 73.67 kHz, force constant 2N/m, oscillation amplitude 2.5 nm.

a) Force "interaction image", total gray scale corresponds to about 1 nN.

b) Frequency "interaction image", total gray scale corresponds to about 300 Hz.

c) Oscillation amplitude "interaction image", total gray scale corresponds to a variation of 0.5 nm (that is about 20% of the total oscillation amplitude). All images have been taken simultaneously with a voltage scan of ±1.5V, and the total tip movement is 100nm. Clearly, the parabolic dependence of interaction on the bias voltage is recognized best in the frequency image for small tip-sample distances.
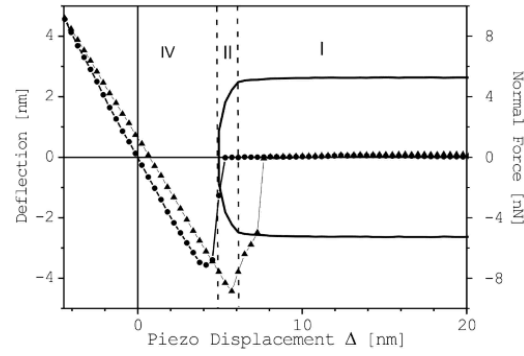
Figure 3
Force vs. distance curve calculated from the force and amplitude *interaction images* shown in Fig. 2. From the force *interaction image* the mean deflection measured by the detection system during the corresponding line of the *interaction image* is shown as solid circles (approach) and triangles (retraction). From the amplitude *interaction image* the oscillation amplitude is calculated and represented as the upper and lower lines in the graph showing the upper and lower turning point of the cantilever during the oscillation. As discussed in the main text, the piezo displacement has been adjusted in order to have the position $\Delta = 0$ at the point where the deflection of the cantilever is zero when tip and sample are in contact. The (apparent) jump distance is about 4 nm and the adhesion force is about 9 nN (=4.5nm x 2N/m). The different interaction regimes described in the main text are separated with dashed lines: (I) "true non-contact regime", (II) "tapping non-contact" and (IV) "continuous contact regime". Due to the soft cantilevers and the low oscillation amplitude used, the "intermittent contact regime" (referred to as region III in the main text) does not appear.
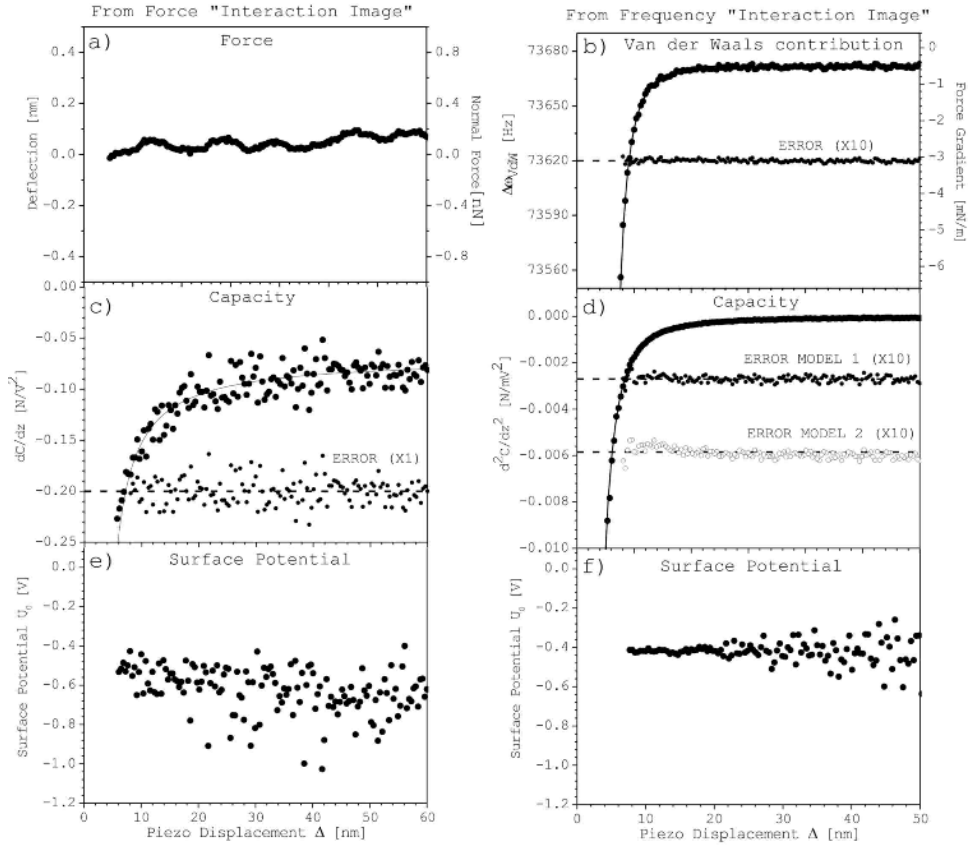

Figure 4
Several interaction vs. distance curves calculated from the force and frequency *interaction images* as discussed in detail in the main text. Graphs b), c) and d) show not only the data points, but also the best fit to the data points

using the relations 9-11 as well as the error to the best fit (smaller points around the dashed horizontal line). For the frequency data, this error is very small, therefore an amplification factor of 10 has been applied as compared to the data points.

Left graphs: Curves calculated from the force *interaction image*: a) Van der Waals force vs. distance curve, c) first derivative of the tip-sample capacitance vs. distance together with the best fit to the data and the corresponding error and e) surface potential vs. distance.

Right graphs: Curves calculated from the frequency *interaction image*: b) Van der Waals frequency vs. distance curve together with the best fit to the data and the corresponding error (x10), d) second derivative of the tip-sample capacitance vs. distance together with the best fit to the data and the corresponding error (x10), and f) surface potential vs. distance. For the capacity data calculated from the frequency *interaction image* (graph d)) the error is shown for two different relations, corresponding to two different descriptions of the tip-sample system. One of the two models (the empty circles) shows a small but clear tendency of the error.

In all graphs, the piezo displacement has been adjusted with the value used in Fig. 3. Note that only data points corresponding to the non-contact regime are shown, therefore no data is shown for tip-sample distances $\Delta < 5$nm. Resonance frequency: 73.67 kHz, force constant 2N/m, oscillation amplitude 2.5 nm.
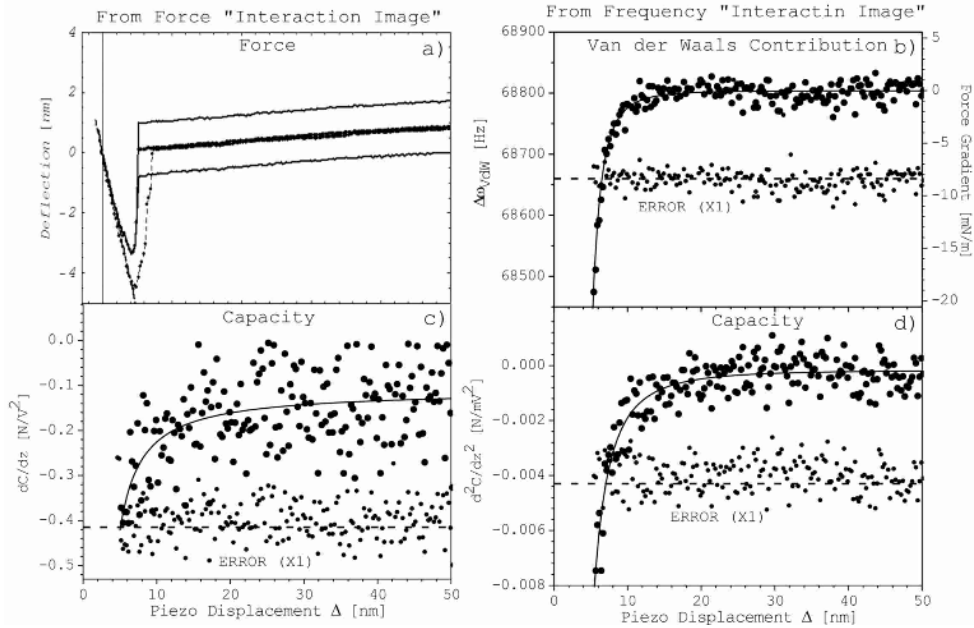

Figure 5

Interaction vs. distance curves calculated from force and frequency *interaction images* (not shown) acquired with a Pt-tip on an Au(111) surface in air. As in Figure 4, graphs b), c) and d) show not only the data points, but also the best fit to these data points using the relations 9-11. The error to the best fit is represented as smaller points around the dashed horizontal line. In this case, no amplification factor has been applied to the errors.

Left graphs: Curves calculated from the force *interaction image*: a) (mean) *FvsD* curve, as in Figure 3 forward and backward cycle are shown. The thicker points correspond to the calculated mean force while the two lines below and over these data points show the oscillation amplitude calculated from the amplitude *interaction image*. Note that, in contrast to figure 3, only the "true non-contact regime" (region I in figure 3) and the continuous contact regime (region IV in figure 3) are measured due to the small oscillation amplitude. c) first derivative of the tip-sample capacitance vs. distance.

Right graphs: Curves calculated from the frequency *interaction image*: b) (Van der Waals) frequency vs. distance curve and d) second derivative of the tip-sample capacitance vs. distance. Resonance frequency: 68.80 kHz, force constant 2N/m, oscillation amplitude 1nm.
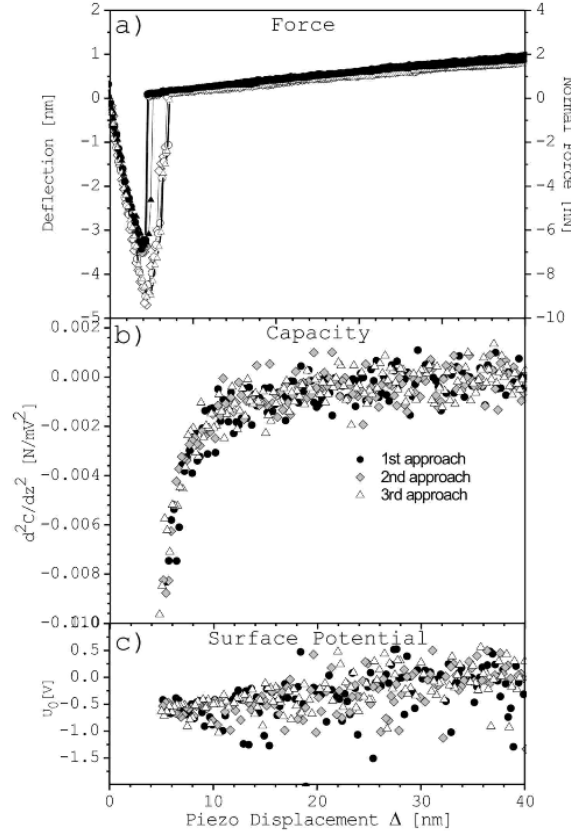
Figure 6

Interaction vs. distance data calculated from three consecutive "interaction images" acquired with a Pt-tip on a Au(111) surface. The data obtained from the three interaction images; the first indentation correspond to circles, the second to diamonds and the third one to triangles. Top image (a): (mean) *FvsD* curve: data corresponding to tip-sample approach and tip-sample retraction is shown. Note that the data corresponding to tip-sample retraction, that is, the part showing adhesion, is represented without filling to aid the eye. Central image (b): Second derivative of tip-sample capacitance obtained from the frequency *interaction images*. Only approach data is shown, the solid circles correspond to the first indentation, the gray diamonds to the second and the white triangles to the third one. Lower image (c): Surface potential calculated from the frequency *interaction images*. Again only approach data is shown and the coding for the different indentations is the same as for graph (b). Resonance frequency: 68.80 kHz, force constant 2N/m, oscillation amplitude 1nm.

IX.   REFERENCES

[1] G. Binnig, C.F. Quate and Ch. Gerber, Phys. Rev. Lett. **56**, 930-933 (1986).
[2] B. Anczykowski, D. Krüger and H. Fuchs, Phys. Rev. B **53**, 15485 (1996).
[3] R.G. Winckler, J.P. Spatz, S. Sheiko, M. Möller, P. Reineker, and O. Marti, Phys. Rev. B **54**, 8908 (1996).
[4] F.J. Giessibl, Phys. Rev. B **56** (24), 16010-16015 (1997).
[5] A. S. San Paulo and R. García, Phys. Rev. B **66**, 041406 (2002).
[6] C.J. Chen, J. Phys. Cond. Matter **3**, 1227 (1991).
[7] C. Argento and R. H. French, J. Appl. Phys. **80**, 6081 (1996).
[8] M. Stark, R.W. Stark, W.M. Heckl and R. Guggenberger, PNAS **99** (13), 8473-8478 (2001).
[9] H.W Gao, A.M. Baró and J.J. Saenz, J. Vac. Sci. Technol **B9**, 1323-28 (1991).
[10] S. Beladi, P. Girard and G. Leveque, J. Appl. Phys. **81** (3) 1023-1030 (1997).
[11] S. Gómez-Moñivas, L.S. Froufe-Pérez, A.J. Caamaño and J.J. Sáenz, Appl. Phys. Lett. **79**, 4048-4050 (2001).
[12] K. L. Sorokina and A.L. Tolstikhina, Crystallography Reports **49**, 476 (2004).

[13] Weisenhorn, A.L, Hansma, P.K and Albrecht, T. R. (1989), Appl. Phys. Lett. **54**, 26, 2651-2653.

[14] T.R. Albrecht, P. Grütter, D. Horne and D. Rugar, , J. Appl. Phys. **69** (2), 668-673 (1991).

[15] U. Dürig, J.K. Gimzewski and D.W. Pohl, *Phys. Rev. Letters*, **57**, (19), 2403-2406 (1986).

[16] Ducker, W. A., Cook, R. F., and Clarke, D. R., *J. Appl. Phys*, **67** (9), 4045-4052 (1990).

[17] B. Gady, D. Schleef, and R. Reifenberger, *Phys. Rev. B* **53**, 8065-8070 (1996).

[18] J. Colchero, A. Storch, M. Luna and A.M. Baró, Langmuir **14**, 2230-2234 (1998).

[19] M. Luna, J. Colchero and A.M. Baró, Appl. Phys. Lett. **72 (10)**, 3461-3463 (1998).

[20] L. Zitzler, S. Herminghaus and F. Mugele, Phys. Rev. B 66, 155436-1 55436-8 (2002).

[21] Here "non-contact" regime refers to the case where tip and sample are neither in mechanical contact nor in very close proximity to the sample, that is, for distances larger than about 1nm in UHV and 2-5 nm in ambient air. For smaller distances chemical forces and -once mechanical contact is established- also elastic forces have to be considered. In addition, in air the interaction due to the formation of liquid necks has to be taken into account. In the present context "true" non-contact regime will refer to the regime where only Van der Waals and electrostatic forces are relevant.

[22] J. Hu, X.D. Xiao and M. Salmeron, Appl. Phys. Lett. **67**, 476-478 (1995).

[23] M. Guggisberg, M. Bammerlin, Ch. Loppacher, O. Pfeiffer, A. Abdurixit, V. Barwich, R. Bennewitz, A. Baratoff, E. Meyer, and H.-J. Güntherodt, Phys. Rev. B, **61**(16), 11151-11155, (2000).

[24] Strictly, only the first and second derivative of tip-sample capacitance are determined, but not the capacitance itself.

[25] To be more precise: the effective force constant $c_{eff} = c - \partial F(d)/\partial d$ of the system should not vary significantly over the range of cantilever oscillation. This implies that $|F''(d_0)| a \ll c_{lever}$, where a is the oscillation amplitude, $F''(d_0)$ the second derivative of the force at the mean equilibrium position d_0, and c_{lever} is the force constant of the cantilever.

[26] Dürig, U., Züger, O. and Stalder, A. (1992), "Interaction Force Detection in Scanning Probe Microscopy: Methods and Applications", J. Appl. Phys., **72**, 1778-1798.

[27] J. Mahanty and B.W. Ninham, "Dispersion Forces", Academic Press, London (1976).

[28] J.N. Israelachvili, "Molecular and Intermolecular Forces", Academic Press, San Diego (1992).

[29] S. Hudlet, M. Saint Jean, C. Guthmann and J. Berger, Eur. Phys. J. **B2**, 5-10 (1998).

[30] J.D. Jackson, "Classical Electrodynamics", 3rd Edition (1999).

[31] S. Gómez-Moñivas, J.J. Sáenz, R. Carminatti, J.J. Greffet, Appl. Phys. Lett. **76**, 2955 (2000).

[32] D.W. Abraham and H.K. Wichramasinghe, J. Vac. Sci. Technol. **B9** (3) 1559-1561 (1991).

[33] J.M.R. Weaver and D.W. Abraham, Appl. Phys. Lett. **58**, 2921-3156 (1991).

[34] J. Colchero, A. Gil, and A.M. Baró, Physical Review B **64** (24), 245403-245413 (2001).

[35] B.D. Terris, J.E. Stern, D. Rugar and H.J. Mamin, Phys. Rev. Lett. **63**, 2669-2662 (1989).

[36] Nanotec Electronica, E-28760 Tres Cantos, www.nanotec.es .

[37] A. Gil, J. Colchero, J. Gómez-Herrero and A.M. Baró, Nanotechnology **14** (2), 332-340 (2003).

[38] S. Sadewasser, Th. Glatzel and M Ch. Lux-Steiner, Applied Surface Science **210**, 84-89 (2003).

[39] G. M. Sacha, A. Verdaguer, J. Martinez, J. J. Saenz, D. F. Ogletree, M. Salmerón, Appl. Phys. Lett **86**, 123101 (2005).

[40] J. Colchero, A. Storch, M. Luna, J. Gómez Herrero and A. Baró, Langmuir, Vol. **18** (9), 716-721 (2002).

[41] Olympus Optical Co. LDT, OMCL-AC series, long cantilevers (length $240\mu m$), nominal force constant: 2 N/m. In our experiments, tips with and without Pt coating have been used. For more information see www.olympus.co.jp/probe .

[42] C. Gómez-Navarro, A. Gil, M. Álvarez, P. J. De Pablo, F. Moreno-Herrero, I. Horcas, R. Fernández, J. Colchero, J. Gómez-Herrero and A.M. Baró, Nanotechnology **13** (3), 314-317 (2002).

[43] C. Gómez-Navarro, F. Moreno-Herrero, P.J. De Pablo, J. Colchero, J. Gómez-Herrero and A.M. Baró, Proc. Nat. Acad. Science **99**, 8484-8487 (2002).

[44] C. Gómez Navarro, A. Gil, M. Alvarez, P.J. de Pablo, F. Moreno-Herrero, I. Horcas, R. Fernandez Sánchez, J. Colchero, J. Gómez-Herrero and A.M. Baró, Nanotechnology **13** (2), 314-317 (2002).

[45] That is, the known piezo calibration is transferred to a calibration of the photodiode by assuming a slope of 1 for the contact regime of the cantilever deflection vs. distance curve. For more details, see ref. [13].

[46] Since $\nu_{cont} \simeq 4.4 \, \nu_{free}$, with our free resonance frequency of $\nu_{free} \simeq 68kHz$ the resoncance frequency in contact is not within the lock range of about $15kHz$ of our PLL).

[47] T. Stifter, O. Marti, B. Bhushan, Physical Review B **62** (20), 13667-13673 (2000).

[48] Prior to the SFM experiments, the Au-(111) surface was flame annealed to remove contaminants. To estimate the contact angle a small drop of water was deposited on an edge of the sample and found to spread, indicating that sample is macrosopically wetting and that the amount of contamination due to hydrocarbons is relatively low.

[49] A. Gil, J. Colchero, M. Luna, J. Gómez and A.M. Baró, Langmuir **16** 5086-5092 (2000).

[50] F.J. Giessibl, S. Hembacher, M. Herz, Ch. Schiller and J. Mannhart, Nanotechnology **15** S79-S86 (2004).

[51] Force data is averaged over a whole "fast-scan" line, where the voltage is varied between $\pm U_{scan}$. Therefore in addition to the Van der Waals interaction, on average also an electrostatic force is acting, since the electrostatic force is proportional to U_{scan}^2, and does not vanish over a"fast-scan" line.

[52] Y. Rosenwaks, R. Shikler, Th. Glatzel and S. Sadewasser, Phys. Rev. B **70**, 085320-1 - 085320-7 (2003).

This figure "Fig1_New.jpg" is available in "jpg" format from:

http://arxiv.org/ps/cond-mat/0602317

This figure "Fig2_New.jpg" is available in "jpg" format from:

http://arxiv.org/ps/cond-mat/0602317

This figure "Fig3_New.jpg" is available in "jpg" format from:

http://arxiv.org/ps/cond-mat/0602317

This figure "Fig4_New.jpg" is available in "jpg" format from:

http://arxiv.org/ps/cond-mat/0602317

This figure "Fig5_New.jpg" is available in "jpg" format from:

http://arxiv.org/ps/cond-mat/0602317

This figure "Fig6_New.jpg" is available in "jpg" format from:

http://arxiv.org/ps/cond-mat/0602317